ARTICLE

Check for updates

Gravity field changes reveal deep mass transfer before and after the 2013 Lushan earthquake

Linhai Wang [1,6], Shi Chen [1,2✉], Jiancang Zhuang[3,4], Bei Zhang[1,2], Wen Shi[1,2], Jinling Yang[1,5] & Weimin Xu[1]

The 2013 M_S7.0 Lushan earthquake, Sichuan, China, occurred on a blind thrust fault in the southern Longmenshan fault belt. The terrestrial hybrid repeated gravity observation enables us to investigate the redistribution of both surface and deep mass. Here, we find a transient increase in the gravity field about 2 years before the earthquake and a drop after the mainshock. A Bayesian inversion method with spatiotemporal smoothness is employed to extract the apparent density changes. The increase of apparent density on the south of the focal zone is assumed to be related to crustal mass transfer. We introduce a disc-shaped equivalent source model with a homogeneous density to address this hypothesis, and estimate the model parameters by Markov Chain Monte Carlo simulations. As a fluid diffusion footprint is indicated by the seismicity migration in this region, with a fitted diffusion rate of $10 \, \text{m}^2 \, \text{s}^{-1}$, we conclude that such deep crustal mass transfer may be caused by fluid diffusion.

[1] Institute of Geophysics, China Earthquake Administration, Beijing 100081, China. [2] Beijing Baijiatuan Earth Science National Observation and Research Station, Beijing 100095, China. [3] The Institute of Statistical Mathematics, Research Organization of Information and Systems, Tokyo 106-8569, Japan. [4] Department of Statistical Science, The Graduate University for Advanced Studies (SOKEN), Tokyo 190-8562, Japan. [5] Fujian Earthquake Agency, Fuzhou 350003, China. [6] Present address: Beijing Baijiatuan Earth Science National Observation and Research Station, Beijing 100095, China. ✉email: chenshi@cea-igp.ac.cn

Spatiotemporal gravity signals from gravity measurement can contribute to the understanding of the surface and subsurface mass redistribution, which reflects the crustal deformation and density changes[1,2]. In the past few decades, the satellite and terrestrial gravity data have been employed to investigate the geophysical process of earthquake[3–5]. Gravity changes derived from satellite gravity measurements may be connected to the pre-seismic signals potentially caused by the deep mass redistribution of the large subduction earthquakes, such as the 2010 M_w8.8 Maule earthquake[5] and the 2011 M_w9.0 Tohuku-Oki earthquake[6,7]. However, the large observation errors of the GRACE satellite gravity[8] and footprints of space gravity data[9] may make it difficult to obtain the local gravity changes with spatial resolution less than several hundred kilometers.

Compared to satellite gravity observation, the Terrestrial Hybrid Repeated Gravity Observation (THRGO) system[4,10] can better solve the problem of spatial limitation. The absolute and relative gravity observations can be periodically performed in local areas. In recent decades, with the rapid development of high-precision absolute gravimetric instruments, the time-varying gravity data obtained by the THRGO system have been employed to investigate the crustal deformation, density change, and deep crustal fluid movement more often in the tectonic active region. In western Europe, low gravity change rates and slow intraplate vertical movements were obtained using repeated absolute gravimetry[11]. With absolute gravity observation data over 20 years in Japan, negative mass anomalies in two recent long-term slow slip events in the Tokai area were reported[12]. The combination of the absolute gravity observation and GPS measurement results reveal the deep mass change and crustal thickening beneath the Tibetan Plateau[13]. In the western China, it is found that the gravity field changed before the 2008 Wenchuan M_S8.0 earthquake in a broad region with the size of about hundreds of square kilometers[14], based on absolute and relative gravity measurement data with an accuracy of ~15 µGal. The gravity increased at four absolute gravimetry stations in the south Tibet near the epicenter of the 2015 Nepal M_w7.8 earthquake, indicating possible mass distribution changes in the broad source region of this earthquake[15]. Using repeated relative gravity observation data in the northeastern Tibetan Plateau, the density variations at different depths over different time before the 2016 M_S6.4 Menyuan earthquake were derived[16].

However, what causes the observed gravity changes and whether these gravity changes can be reliably used in the earthquake precursor research is still under debate. The arguments mainly focus on the factors affecting the measurement results of absolute and relative gravimetry, such as instrumental artifacts, hydrogeological effects, and topography deformations[17,18]. It is well known that the surface observable gravity changes related to seismic tectonic movement in deep crust are characterized by low signal-to-noise ratios[19]. Consequently, whether the observed gravity change has an enough signal-to-noise ratios for investigating the tectonic movement is still a great challenge. The observed gravity changes at Pixian absolute gravimetry station before the 2008 Wenchuan M_S8.0 earthquake using absolute gravimetric with a high signal-to-noise ratios were obtained[20]. It is found that the corrected residual gravity changes were much larger than the possible gravity effects due to vertical deformation and hydrological processes. Their results provided an insight on interpreting the mechanisms of deep mass changes. In terms of geodynamic numerical simulation, it is suggested the presence of observable yearly transient change in gravity related to the movement of deep fluids[21]. Therefore, by means of the THRGO, it is possible to isolate the gravity signals potentially related to the deep mass migration.

In this study, we investigate the gravity change from absolute and relative gravity observations before and after the 2013 Lushan M_S7.0 earthquake. The mainshock occurred on a blind revers-fault in the Longmenshan fault belt in the eastern Tibetan Plateau. The Longmenshan thrust belt is formed by the crustal shortening of the eastern margin of the Tibetan Plateau Block, which collides with the South China Block in Fig. 1a. The 2008 Wenchuan M_S8.0 earthquake occurred in the middle north section of the Longmenshan fault zone in Sichuan Province, China. Almost five years after the Wenchuan earthquake, the Lushan M_S7.0 earthquake occurred on April 20, 2013, another devastating earthquake along the southern section of the Longmenshan thrust belt as shown in Fig. 1b. However, unlike the Wenchuan earthquake, the Lushan M_S7.0 earthquake occurred on a blind revers-fault, with no obvious surface rupture or crustal displacement found around the epicenter[22]. Then, the mechanism generating the Lushan earthquake remains debated, for example, whether it was a triggering effect[22,23], or an aftershock[24,25] of the M_S8.0 Wenchuan earthquake.

As shown in Fig. 1c, the Sichuan hybrid gravity observation network consists of 3 absolute gravity observation stations and 142 relative gravity observation stations. The epicenter of the M_S7.0 Lushan earthquake was in the northern section of the Sichuan THRGO network. Several previous studies have reported gravity changes before the M_S7.0 Lushan earthquake based on the THRGO dataset[26–28]. However, how the gravity change relates to the mechanism of the Lushan earthquake occurrence remains debated. Therefore, we try to isolate the gravity signals that are potentially related to deep tectonic movements, and the seismogenic environment of the Lushan earthquakes.

The following sections are organized as follows. First, we show the time series of absolute and relative gravity data, and obtain the apparent density of the deep source. Second, we use the equivalent source model (ESM) to estimate the deep source mass change parameters in the region with gravity changes. We also give the geodynamic interpretation of the equivalent source inversion results as well as the related evidence from other geophysical observations. Third, we summarize our findings and present our concluding remarks. At last, we introduce the processing and quality control of the gravity observation data, and the state-of-the-art method on the apparent density inversion and ESM inversion.

Results

Time series of absolute and relative gravity data. The absolute gravity observation is carried out at the Pixian absolute gravity stations once to twice a year from 2008 to 3013. Figure 2a shows that the gravity at Pixian station decreases from 2008 to 2011 after the 2008 Wenchuan M_S8.0 earthquake, and then increase from 2011 to 2013 before the 2013 Lushan M_S7.0 earthquake. The time series of Xichang and Panzhihua absolute gravity stations with the accuracy of those values is better than 5 µGal (details as Supplementary Fig. 1). Since August 2010, the Sichuan Earthquake Agency has used two LaCoste and Romberg Model G relative gravimeters to conduct THRGO in the Sichuan Gravity Survey Network with the back-and-forth repeated observation method for all loop surveys. The gravity survey campaign was carried out twice a year, with the first survey lasting from April to May and the second one from August to September. To study the changing process of time-lapse gravity before and after the 2013 M_S7.0 earthquake, we use the Modified Bayesian gravity adjustment (MBGA) method[29,30] (details in "Methods") to process the seven THRGO datasets. The six epochs cumulative changes of gravity value using the gravity values of August, 2010 as the time reference were obtained. As shown in Fig. 2b–g. In general, the
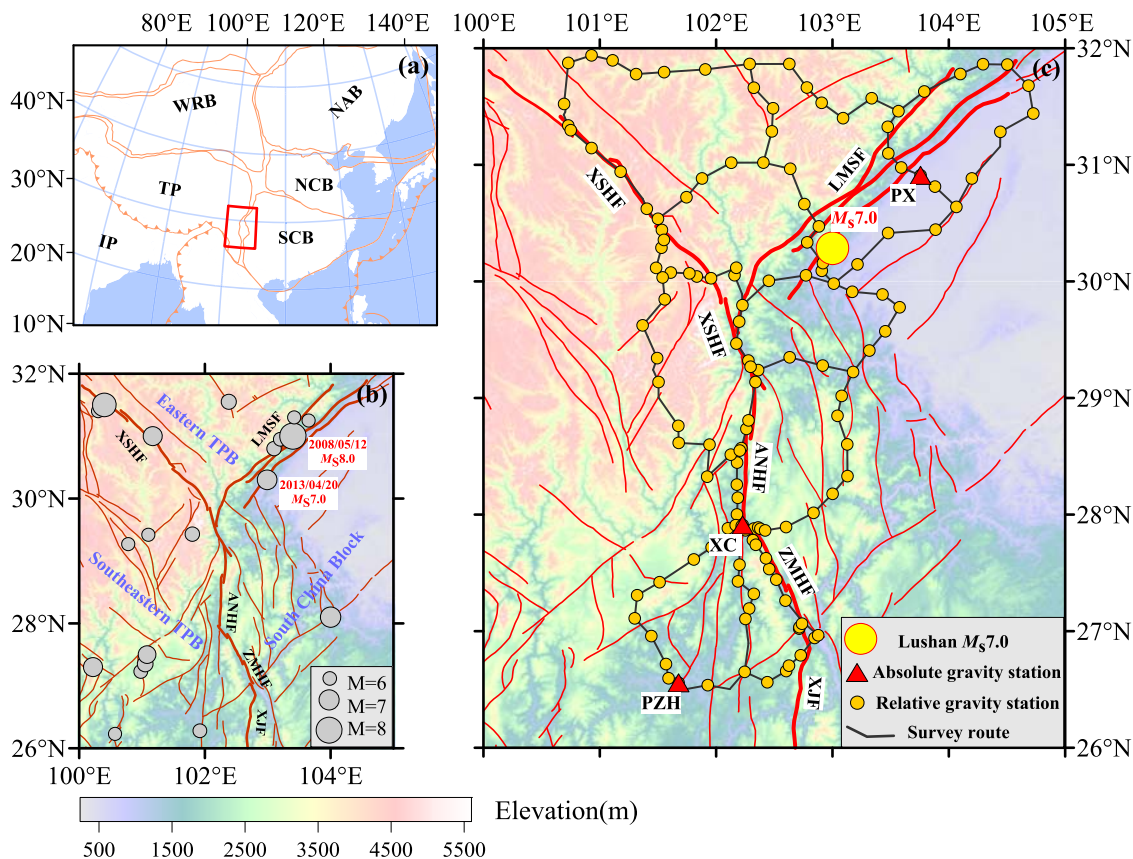
Fig. 1 Tectonic settings and gravity survey network in Sichuan, China. a Geographical position of the study area is marked by the red rectangle (WRB: West Region Block; NAB: Northeast Asia Block; NCB: North China Block; SCB: South China Block; TP: Tibetan Plateau; CBB: China–Burma Block; IP: Indian Plate). **b** The gray circles mark the earthquakes with magnitude greater than $M_S 6.0$ during 1970–2013.4.20 from the China Earthquake Network Center catalog. The topography in this study is from the Shuttle Radar Topography Mission (https://srtm.csi.cgiar.org/srtmdata/). **c** The light yellow circle represents the epicenter location of the 2013 Lushan $M_S 7.0$ earthquake. The thick red lines represent the major faults (ANHF: Anninghe Fault; XJF: Xiaojiang Fault; LMSF: Longmenshan Fault; ZMHF: Zemuhe Fault; XSHF: Xianshuihe Fault.). The dark yellow dots and black lines denote the stations and survey routes of relative gravity observation, respectively. The red triangles indicate the locations of the absolute gravity stations (Pixian PX, Xichang XC, Panzhihua PZH). The locations of gravity stations are available in the supplementary material in the data repository.

gravity changes range from −60 to 90 µGal and the accuracies of gravity values at each measured stations are within 15 µGal, with an average value of 7.4 µGal.

Apparent density modeling. The six epochs cumulative gravity changes are used as input observation data for the BADI method[31,32] (details in "Methods") to calculate the cumulative changes in the source apparent density. The results in Fig. 3 indicate that the inverted deep source apparent density locates in the well-resolution region of the Sichuan gravity network (outlined by the gray dotted line), over which the inversion results are more accurate (see Supplementary Fig. 2) than the other regions. The inverted apparent density ranges from −1.5 to 2 kg m^{-3} (in Fig. 3). Figure 3a–d shows that the increase of apparent density before the Lushan earthquake in the southern epicenter of Lushan $M_S 7.0$ earthquake, ranges from 0.5 to 2 kg m^{-3}. The area with apparent density increase distributes in a range of about 300 km in the N-S direction and 150 km in the E-W direction. After the Lushan earthquake, the apparent density gradually shrinks (in Fig. 3e, f).

Model-assimilated time-varying gravity field. The apparent density model can be considered as the field source of gravity changes with the regional and trend processes. The model-assimilated gravity changes can be derived from this equivalent

apparent density model. Figure 4 shows the cumulative model-assimilated gravity change calculated by forwarding the field source apparent density in Fig. 3. Compared to the six epochs cumulative changes of the adjusted gravity value obtained by the MBGA method (Supplementary Fig. 3a–f), the high-frequency components in the gravity change calculated by the BADI method are obviously reduced. In Fig. 4, the model-assimilated time-varying gravity field increase before the earthquake (Fig. 4a–d) and gradually decreases after the earthquake (Fig. 4e, f) in the southern epicenter of Lushan $M_S 7.0$ earthquake (the area within the black dotted line).

We compare the gravity changes obtained by MBGA and BADI method at selected gravity stations inside (WSH, EB, DJY) and outside (KD, XJ, DJY) the area in Fig. 4g, h. Compared with the results obtained from the BADI method (Fig. 4h), the gravity changes obtained by MBGA method (Fig. 4g) are generally larger and do not have a stable changing trend. In Fig. 4h, the maximum gravity changes in EB, LC, and WSH generally show the increase rate of about 23 µGal year^{-1} (µGal yr^{-1}) and decreasing before and after the earthquake, respectively, while those in DJY, XJ, KD do not have such trends.

The hydrological signal and crustal deformation. As shown in Figs. 4a–d, the model-assimilated time-varying gravity field at the gravity stations south of the epicenter show a maximum growth
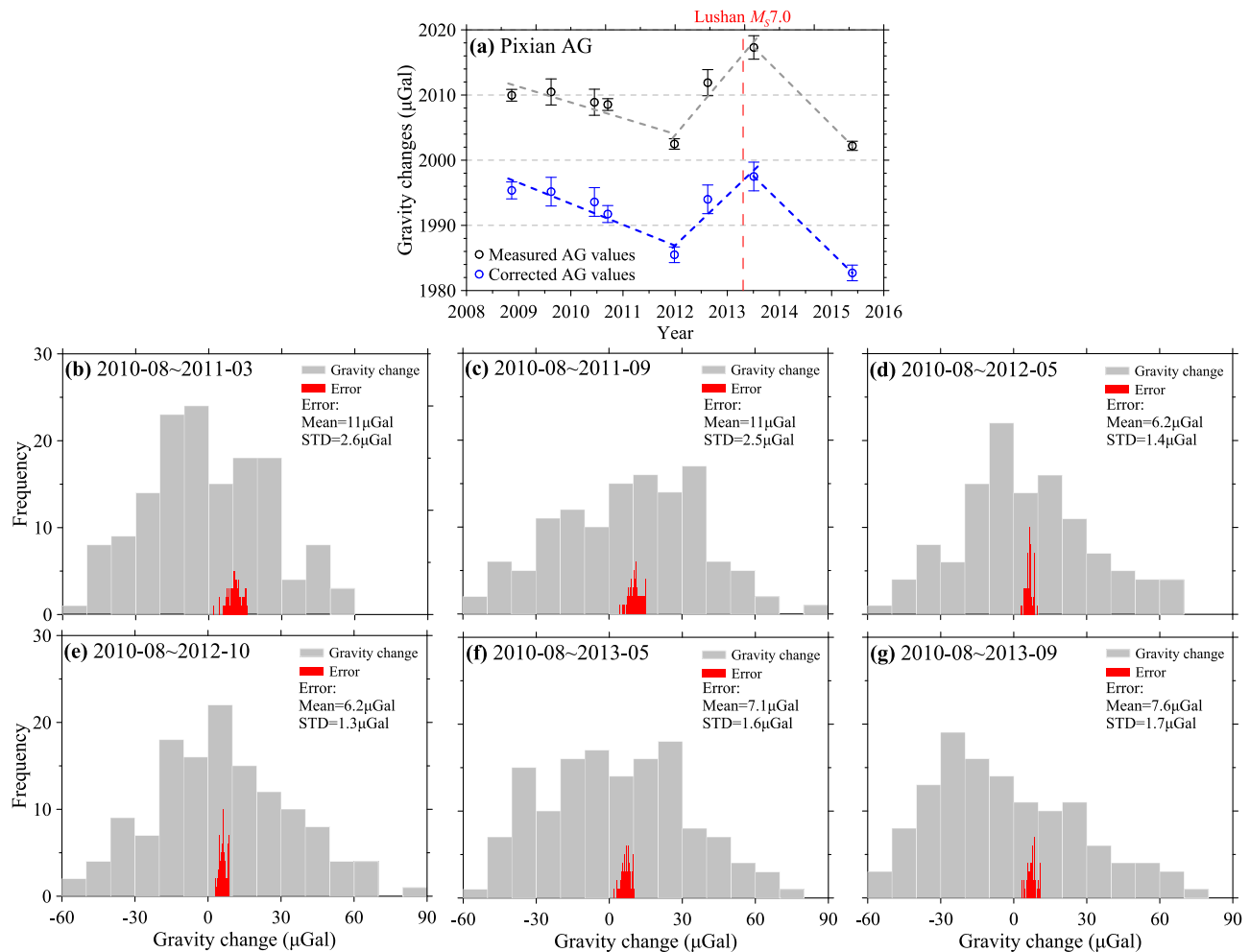
Fig. 2 The time series of absolute and relative gravity observation. a The time series of Pixian absolute gravity (AG) observation. The gray and blue error bars represent absolute gravity measurement errors and correction errors, respectively. **b–g** Six epochs gravity changes and errors obtained using the MBGA method. In (**a**), the gray and blue dot, respectively, indicated the observed data and corrected data after correcting the total terrestrial water storage and vertical displacement. The constant value is, respectively, removed for the reading.

rate of 23 µGal yr^{-1} before the Lushan M_S7.0 earthquake. What is the main reason for this gravity increase, for example, the environmental noise from surface gravity observations or the migration of mass in the deep crust, requires further verification.

First, the gravity effect due to surface and subsurface water level changes should be considered. To estimate the gravity effect of groundwater change, we collected the monthly groundwater storage from the WaterGAP Global Hydrology Model (WGHM)[33]. The gravity change caused by groundwater change, $\triangle g_{GW}$, can be quantified with a linear model[20]: $\triangle g_{GW} = r * \Delta H * 0.042$ µGal mm^{-1}, where r is the porosity and ΔH is the change level of groundwater. Figure 5a shows the gravity decrease rate of -0.3 µGal yr^{-1} in the south area of Lushan epicenter, and a maximum decrease rate of -0.6 µGal yr^{-1} in the Chengdu city. The Water Resources Bulletin (WRB) of the Sichuan (Water Resources Bulletin of Sichuan in 2010, 2011, 2012, and 2013) from 2010 to 2012 provides only an annual regional average of groundwater recourses, with a decrease of groundwater since 2010. These could cause underestimation of the observed gravity increase before the earthquake. The trend of groundwater change from the WGHM model is generally consistent with the WRB data.

To estimate the gravity effect caused by the terrestrial water storage change, we collect the GLDAS data-Noah land surface

model[34] with $0.5° \times 0.5°$ in the month corresponding to the relative gravity observation. We calculate the gravity effect from 2010 to 2012 using the 'Soil moisture (0–10 cm,10–40 cm, 40–100 m, and 100–200 cm)', 'Snow depth water equivalent' and 'Plant canopy surface water' in the GLDAS_Noah model. We find that the maximum decrease rate of equivalent water height in the south area in the Lushan epicenter from 2010 to 2013 is approximately -12 mm/yr, which results in a Bouguer gravity change of -0.5 µGal yr^{-1} in Fig. 5b.

To verify the actual hydrological change, we also collected the hourly precipitation observation data of surface meteorological stations in China from China Meteorological Data Network (http://data.cma.cn/). First, we calculate the annual rate of change of precipitation after excluding evaporation. Then, we find the maximum decrease rate of residual precipitation in the south area of the Lushan epicenter from 2010 to 2012 is approximately -17 mm/yr, which results in a Bouguer gravity change of -0.7 µGal yr^{-1} in Fig. 5c. The results are consistent with the drought[35,36] during the winter of 2011 to 2012.

To analyze the results of the GRACE satellite counterpart for mass migration in this region[9], based on the CSR Release-06 GRACE level-2 data products, we obtain and process time series of monthly time-variable gravity field using the DDK6 filtering method. The gravity change rate from September 2010 to
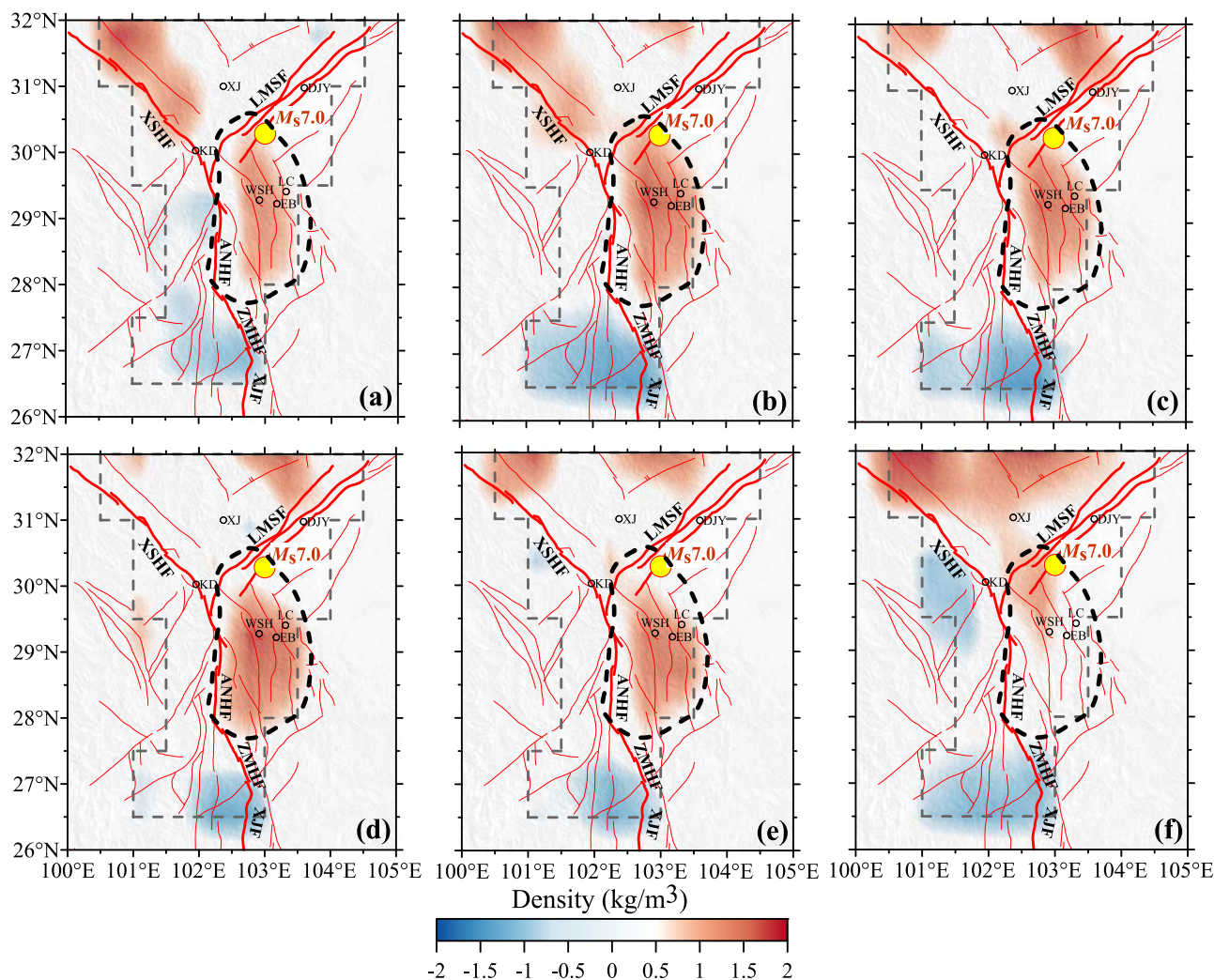
Fig. 3 The cumulative change of the deep source apparent density before and after the Lushan M_S7.0 earthquake obtained by the BADI method. Before the earthquake: **a** 2010-08 ~ 2011-03, **b** 2010-08 ~ 2011-10, **c** 2010-08 ~ 2012-05, **d** 2010-08 ~ 2012-10; after the earthquake: **e** 2010-08 ~ 2013-05, **f** 2010-08 ~ 2013-09; XJ: Xiaojin, DJY: Dujiangyan, KD: Kangding, WSH: Wusihe, LC: Longchi, EB: Ebian. The gray dotted line marks the area where the apparent density can be inverted more accurately. The black dotted line marks the area where the apparent density has a stable change trend.

November 2012 is shown in Fig. 5d. In the study area, the south-central region shows a large range of gravity reduction up to $-3.6\,\mu\text{Gal yr}^{-1}$, while the gravity increase in the northwest and east part of the study area can reach $0.6\,\mu\text{Gal yr}^{-1}$. It is noted that the gravity change observed by GRACE is consistent with the overall change trend of gravity change calculated based on the precipitation data of surface meteorological stations in Fig. 5c, especially in the southern and northwest edges of the study area. However, the magnitude of gravity changes from GRACE satellite measurement due to high order truncation error of the model are lower than the gravity changes observed by terrestrial observation in this study.

Moreover, we quantitatively estimate the potential gravity contribution of crustal vertical deformation in this area. We collect the vertical velocity from GPS measurement[37], and find that most of the areas south of the Lushan epicenter are undergoing surface uplift[38,39]. Figure 5e shows that the uplift rate is up to about 3 mm/year, which could produce a gravity change of about $-1\,\mu\text{Gal yr}^{-1}$ according to the free-air gravity gradient of $0.3086\,\mu\text{Gal mm}^{-1}$. Similarly, the surface subsidence rate in the local areas is about $-4\,\text{mm yr}^{-1}$, which indicates a free-air gravity change of about $1.2\,\mu\text{Gal yr}^{-1}$.

Therefore, the gravity changes of terrestrial water storage and crustal vertical deformation are about $-2\,\mu\text{Gal yr}^{-1}$, which are not enough to well explain the gravity increase up to about $23\,\mu\text{Gal yr}^{-1}$. We infer that the gravity increases south of the epicenter before the 2013 M_S7.0 Lushan earthquake may be related to the deep mass transfer controlled by the tectonic movement in the seismogenic region.

Discussion

Since the model-assimilated time-varying gravity field cannot be well explained by known causes, we need to further quantify the deep source mass. Moreover, as shown in Fig. 4, there are several abnormal areas with gravity change, which results in uncertainty in the spatial distribution analysis of the gravity change. However, the gravity changes in the area south of the Lushan epicenter show the largest gravity increase before the earthquake and decreasing after the earthquake. This trend may conform the characteristics of deep tectonic movements. In this typical region, with the driving force of tectonic movement assumed, a quantitative model of crustal equivalent mass migration associated with dynamic apparent density changes needs to be proposed.
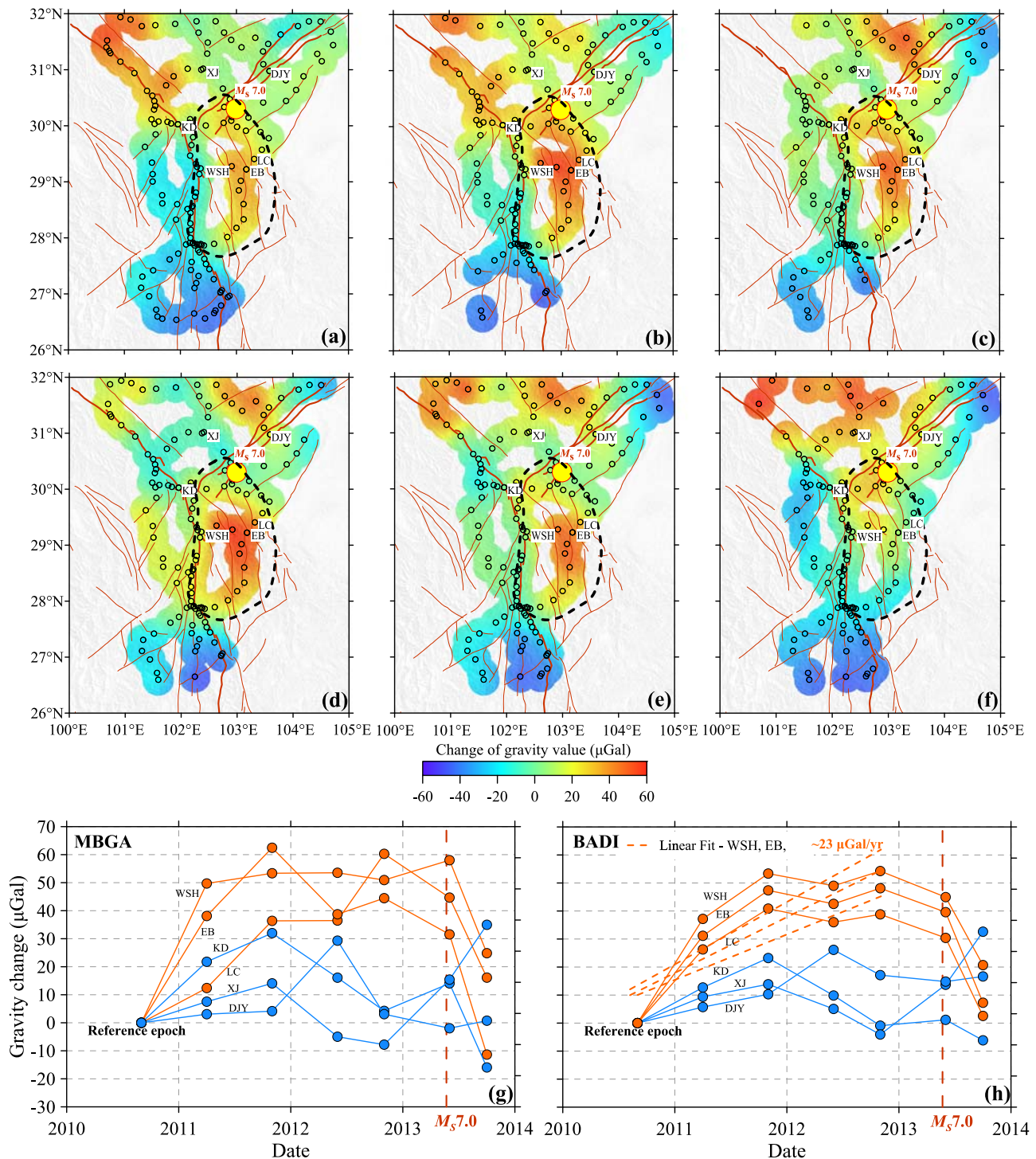
Fig. 4 The cumulative model-assimilated gravity changes calculated from the deep source apparent density. Before the earthquake: **a** 2010-08 ~ 2011-03, **b** 2010-08 ~ 2011-10, **c** 2010-08 ~ 2012-05, **d** 2010-08 ~ 2012-10; after the earthquake: **e** 2010-08 ~ 2013-05, **f** 2010-08 ~ 2013-09. The black dotted line marks the area where the gravity changes increase. **g, h** The gravity changes, respectively, obtained by MBGA and BADI method at selected gravity stations inside (orange dotted) and outside (blue dotted) the area.

Equivalent source model. The hypothesis of 'subsurface mass transfer' and the 'hypocentroid' model have been proposed to explain the gravity change before large earthquakes[15,40,41]. First, according to the hypothesis of 'subsurface mass transfer', the migration of deep crustal mass (fluid) driven by tectonic stress could cause equivalent mass source change related to the occurrence of earthquakes. Then, like the concepts of hypocenter and epicenter in seismology, 'hypocentroid' and 'epicentroid'[42] are

introduced to quantify the range of the deep equivalent mass transfer. The 'hypocentroid' is the center of the equivalent mass source and the projection of the 'hypocentroid' on the ground is the 'epicentroid'.

In this study, we assume that the gravity increase in the southern epicenter of the Lushan $M_S7.0$ earthquake is caused by deep crustal mass migration due to tectonic movement. We use a disc-shaped source model with uniform density to simplify the
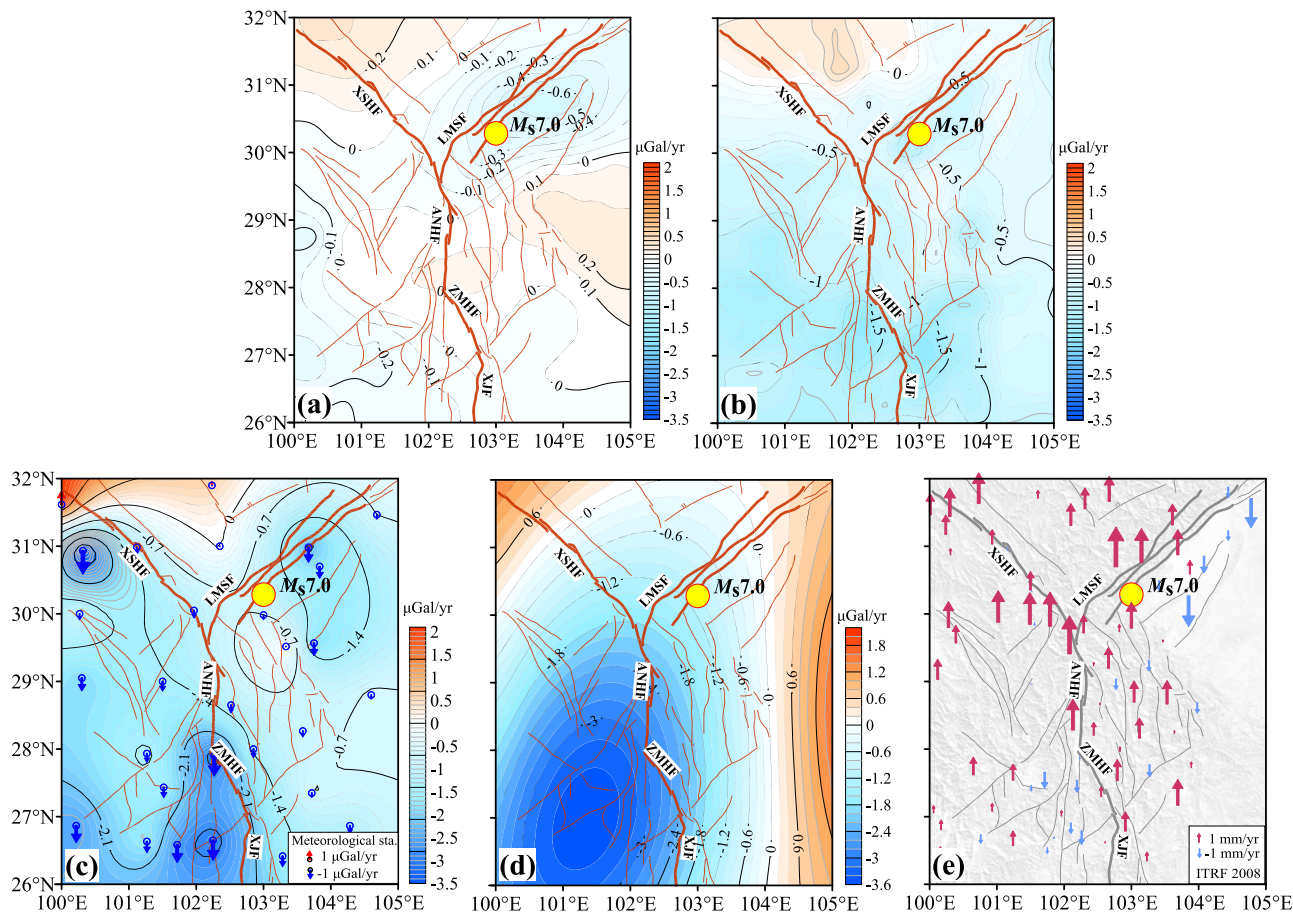
Fig. 5 The hydrological gravity effect and vertical deforamtion in the study area. a The gravity change rate associated with the groundwater level change from WGHM model. **b** The gravity change rate related to the terrestrial water storage from GLDAS. **c** The gravity change rate caused by the precipitation change. **d** The gravity change rate from the GRACE satellites gravity measurement. **e** The vertical velocity from the continuous GPS measurement. The position of blue arrow in (**c**) indicates the location of the meteorological station.

Table 1 Comparison of the disc-shaped model parameters obtained using the gravity change rates from the MBGA and BADI method.

Data	Depth (km)	Radius (km)	Thick (km)	Latitude (°)	Longitude (°)
MBGA	26.8 ± 2.7	87.5 ± 2.3	0.7 ± 0.1	29.3 ± 0.10	103.3 ± 0.02
BADI	26.3 ± 2.6	82.0 ± 1.2	0.7 ± 0.1	29.2 ± 0.03	103.3 ± 0.01

simulation of equivalent mass change in the deep crust, which can quantify the range of the deep equivalent mass transfer. Then, the disc-shaped model is used to parameterize the 'hypocentroid' and 'epicentroid' model[15,42], calling 'equivalent source model' (ESM). The parameters of ESM include the center of the disc-shaped source (i.e., 'hypocentroid') and its projection on the ground (i.e., 'epicentroid').

Gravity changes caused by the ESM can be calculated using the method of horizontal circular discs[43] (see Supplementary method 2). Based on the gravity change results before the Lushan Ms7.0 earthquake, we adopt the Markov Chain Monte Carlo (MCMC) method[44] to estimate the disc-shaped equivalent source model parameters and quantify the uncertainty of those parameters (details in Methods). Using gravity data from the stations south of the epicenter (the area within the black dotted line) in Fig. 4, we calculate two sets of annual gravity change rate from the MBGA method and BADI method through linear fitting of five periods of observation before the Lushan earthquake, respectively. Then, those two sets of annual rates are used to

invert the disc-shaped source model. The two inversion results are listed in Table 1. Compared to the result associated with the MBGA method, the disc-shaped model obtained based on the BADI method has smaller uncertainty.

To analyze the spatial correlation of gravity changes with the inverted disc-shaped model, we calculate the distances between gravity stations and the epicentroid of the equivalent source. Then, we compare the two sets of gravity change rates obtained using the MBGA and BADI method with the corresponding theoretical gravity change rates produced by the two disc-shaped models, as shown in Fig. 6a, b. Figure 6a, b shows that the gravity change rate that locates in the distance less than the corresponding inversed radius has an inverse relationship with the distance away from the epicentroid. Compared to the results from the MBGA method, the spatial distribution of the gravity changes rates obtained by the BADI method is more consistent with the gravity changing trend produced by the theoretical disc-shaped model. The inverted residuals (Fig. 6a) from the MBGA method can reach −16 to 13 μGal, while the residuals from the BADI
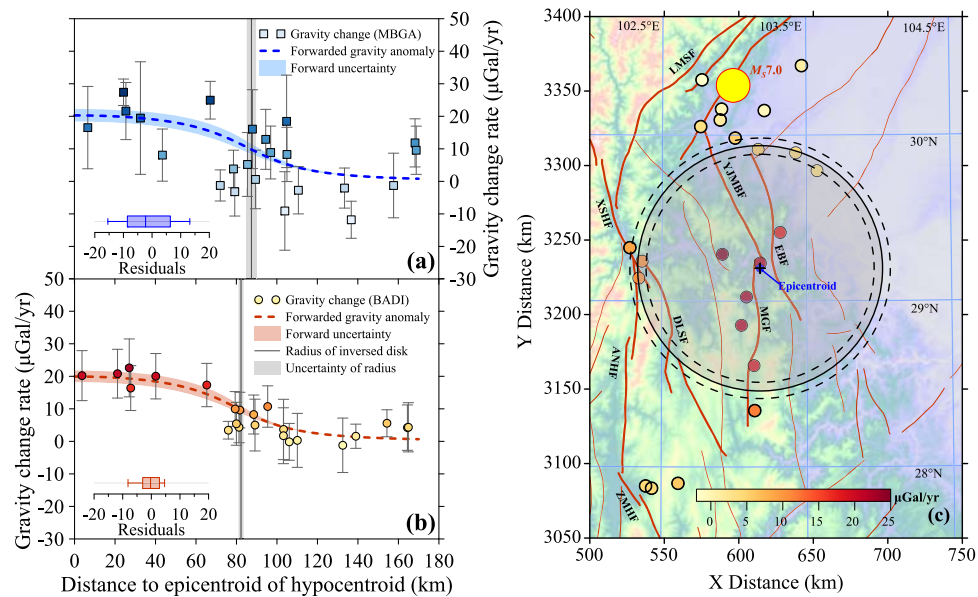
Fig. 6 The relationship between different gravity change rates and corresponding disc-shaped model. a and **b** are gravity change rates, respectively, derived from the MBGA method and BADI method versus the distance away from the epicentroid of hypocentriod; **c** 'hypocentroid' and 'epicentroid' model constructed using the disc-shaped model parameters obtained from the BADI method. In **a** and **b**, the gray shaded area is the uncertainty in the radius of the inverted disk, the gray vertical line is the inverted mean radius. The gray error bar represents the fitting error. In **c**, the gray solid and dashed lines are the radius of the disk model and the uncertainty in the radius, respectively. DLSF: Daliangshan Fault; JPF: Jinping Fault, YJMBF:Yingjingmaba Faul; MGF: Meigu Fault; EBF: Ebian Fault.

method (Fig. 6b) is smaller, ranging from −8 to 5 μGal. Moreover, compared to the results from the MBGA method, the uncertainty in the radius (Fig. 6b) obtained by the BADI method is also smaller. However, the gravity change rate at the gravity stations outside the radius may be mainly affected by the deep mass migration of other regions (detailed as Supplementary Fig. 4). In this study, we selected the region with the largest magnitude and continuous increase of gravity change for modeling. In Fig. 6c, the disc-shaped model parameters obtained using the gravity change rates derived from the BADI method are used to construct the 'hypocentroid' and 'epicentroid' model. The maximum gravity rate near the center of the disc-shaped model is about 20 μGal, which is consistent with the gravity change forwarded by the horizontal disc model[20].

Evidence from other independent observations. To verify whether the gravity increase before the M_S7.0 Lushan earthquake is related to the migration of deep crustal mass transfer in the disc-shaped source region, other independent evidence should be found. In the following, we investigate the regional seismicity, geophysical and geochemical observations in this region, and use them to verify our equivalent source model.

The regional seismicity. The movement of fluids material at various depths in the crust is one of the most likely sources of the gravity change, and often triggers anomaly seismicity[45,46]. Numerous previous studies proposed that some earthquake swarms before or after the mainshock might be associated with the migration of crustal fluids[47–50]. To analyze the spatiotemporal distribution of earthquake events in the disc-shaped source region before the Lushan M_S7.0 earthquake, we make use of the relocated earthquake catalog issued by China Seismic Experimental Site. The catalog from 2009 to April 2013 (before the Lushan earthquake) in the region of 102°E–104°E and 28°N–30.4°N is selected, which covers the disc-shaped source and the Lushan earthquake epicenter. The minimum magnitude of completeness

estimated using the G-R relationship for this catalog is M_S1.9. Figure 7a plots the projection of the disc-shaped model in the ground surface and the seismic events with magnitudes greater than M_S2 and depths greater than 10 km are drawn. Besides the earthquake accumulation at the intersection of XSHF, ANHF, and DLSF in the west, the seismic events are mainly located in the northern part of the disc-shaped model. In Fig. 7a, the earthquakes north of the center of the disk (shown in the blue shaded area) are closer to the epicenter of Lushan earthquake than the earthquakes south of the center of the disk (shown in the green shaded area). The distance from the selected earthquake epicenter to the epicentroid of the disc-shaped equivalent source model is defined as epicentroid distance. Figure 7b, c, respectively, shows the correlation between the epicentroid distance, the focal depth and the occurrence time of earthquake north of the center of the disk in Fig. 7a. Figure 7d, e describes the characteristic of the earthquake distribution south of the center of the disk.

As shown in Fig. 7b, c, from August 2010 to April 2013, the epicenters of the selected earthquakes show a migration beginning at an epicentroid distance of ~30 km and depth of ~26 km. This migration conforms the spatiotemporal feature of fluid diffusion equation. Based on the fluid diffusion formula $D = r^2/4\pi t$, three diffusion rates (8, 10, 12 m^2 s^{-1}) are selected to plot the three diffusion curves in Fig. 7b, and r and t are the calculated distance and time from the epicentroid[48,51]. The distance for the most of earthquakes must be smaller than the values given by the diffusion formula. The corresponding curve could be an upper bound of the multitude of points[51]. The smallest fluid diffusivity in Fig. 7b that can cover almost all the seismic events is estimated to be ~10 m^2 s^{-1}. As shown in Fig. 7d, e, from August 2010 to April 2013, the epicenters of the selected earthquakes show a migration beginning at an epicentroid distance and ~70 km and depth of ~26 km. The fitted rate of fluid diffusion is about 6 m^2 s^{-1}.

There are several studies on earthquake swarms in the lower crust in the previous literatures. In Long Valley Caldera, California, USA, the hypocenters of the 2009 earthquake swarm
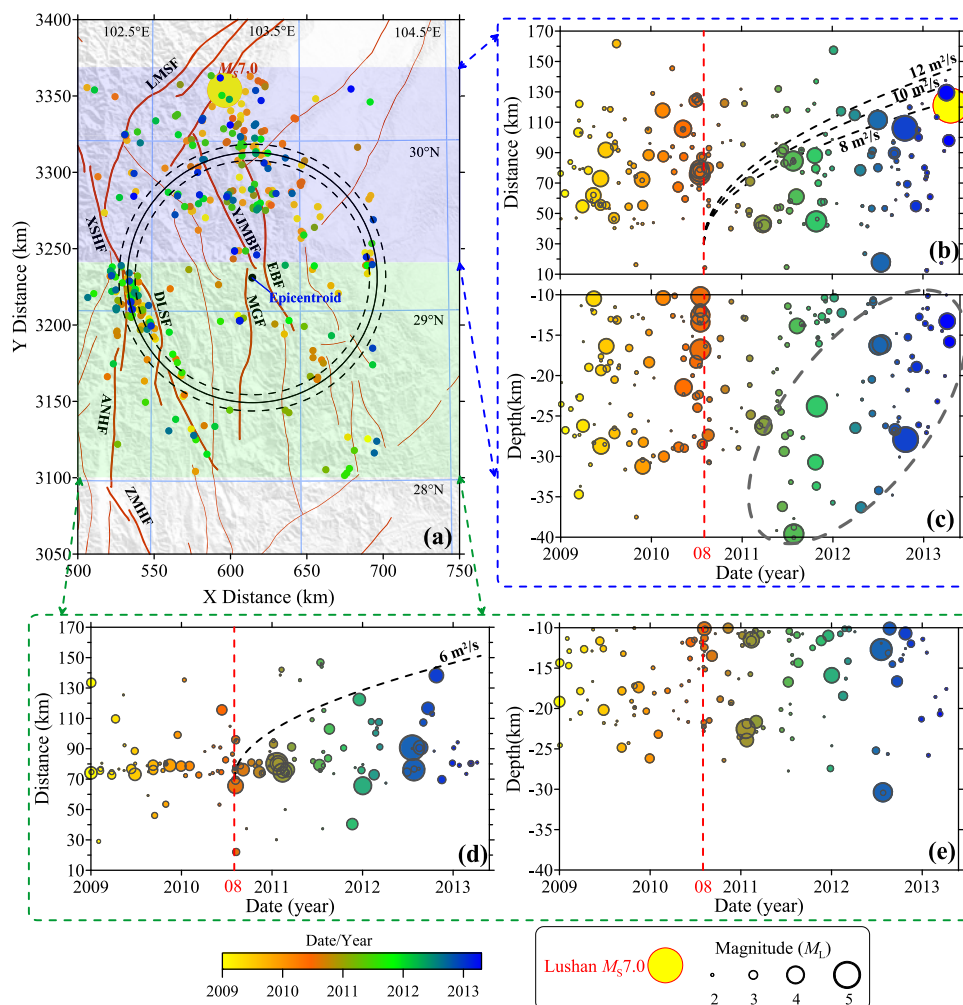
Fig. 7 The spatiotemporal characteristics of earthquake catalog before Lushan M_S7.0 earthquake. a Distribution of earthquakes with focal depths greater than 10 km and magnitudes greater than M_S2; Figure **b** and **c**, respectively, shows the correlation between the epicentroid distance, the focal depth and the occurrence time of earthquake within the blue shaded area in (**a**), while **d** and **e** describes characteristic of the earthquake distributed in the green shaded area. The vertical axis of the three black curves is the ordinate axis on the left. The common unit of diffusion rate is m² s⁻¹, which has been converted into km in the calculation.

migrated upward from depths of 21 to 19 km over ~12 h. The relatively high migration rate suggests that the CO_2-rich hydrous fluids might be a trigger for the 2009 swarm[52]. Beneath Harrat Al-Madinah in Saudi Arabia, the 1999 seismic swarm was triggered when a low-velocity reservoir at depth of 20–40 km was recharged by an intruding magmatic material from a deeper source, possibly the deeper low-velocity zone[53].

Geochemical and seismological observations. The ³He/⁴He, CH_4, and CO release data can also provide an insight on the deep fluid mass transfer and indicate the potential tectonic activity. Previous studies have reported that the CH_4 and CO emission anomalies obtained from NASA's Aqua satellite before the M_S7.0 Lushan earthquake are obviously distributed along the active faults, such as the southern LMSF, XSHF, YJMBF, and JPF fracture zones[54,55], as shown in Fig. 8a. Moreover, the statistical results from published studies show that both the observed ³He/⁴He values and crustal uplift rate are high in the Kangding-Moxi (KD-MX) region (Label in Fig. 8a), implying that there are deep mantle-scale dynamic processes[56] beneath southeastern XSHF (shown in Fig. 8a). The Sichuan Basin and the ANHF-ZMHF-XJF region have lower ³He/⁴He values (mostly less than 0.10 RA)[56].

Recent seismic tomography results show that low-velocity zones (LVZ) are widely distributed in Sichuan Yunnan region, which becomes the transmission, concentration, and accumulation area of stress and strain with its edge area being prone to earthquakes[57–59]. The SWChinaCVM-1.0 model[60] is a recent 3D P-wave and S-wave seismic velocity community models of the crust and upper mantle in Southwest China. In Fig. 8b, d, we show P wave velocities along profiles AA′, BB′, and CC′ passing through hypocentroid of the disc-shaped source model and the hypocenter of the Lushan earthquake, with the earthquakes occurred from August 2010 to April 2013. In Fig. 8b, the profile of AA′ along 103.3°E show that the disc-shaped source region (the black dashed box) locates in an obvious low-velocity zone. Moreover, the earthquakes are primarily distributed in the high-low-velocity boundary (HLVB). The occurrence depth extends from approximately 26 to 45 km, and then moves upward to near the hypocenter area of the M_S7.0 Lushan earthquake. The results of section BB′ along 29.2°N show that the disc-shaped source area is low-velocity zone compared with the east and west sides (Fig. 8c). The profile CC′ (along 30.3°N) shows the hypocenter of Lushan earthquake locates in the HLVB beneath the LMSF (Fig. 8d).
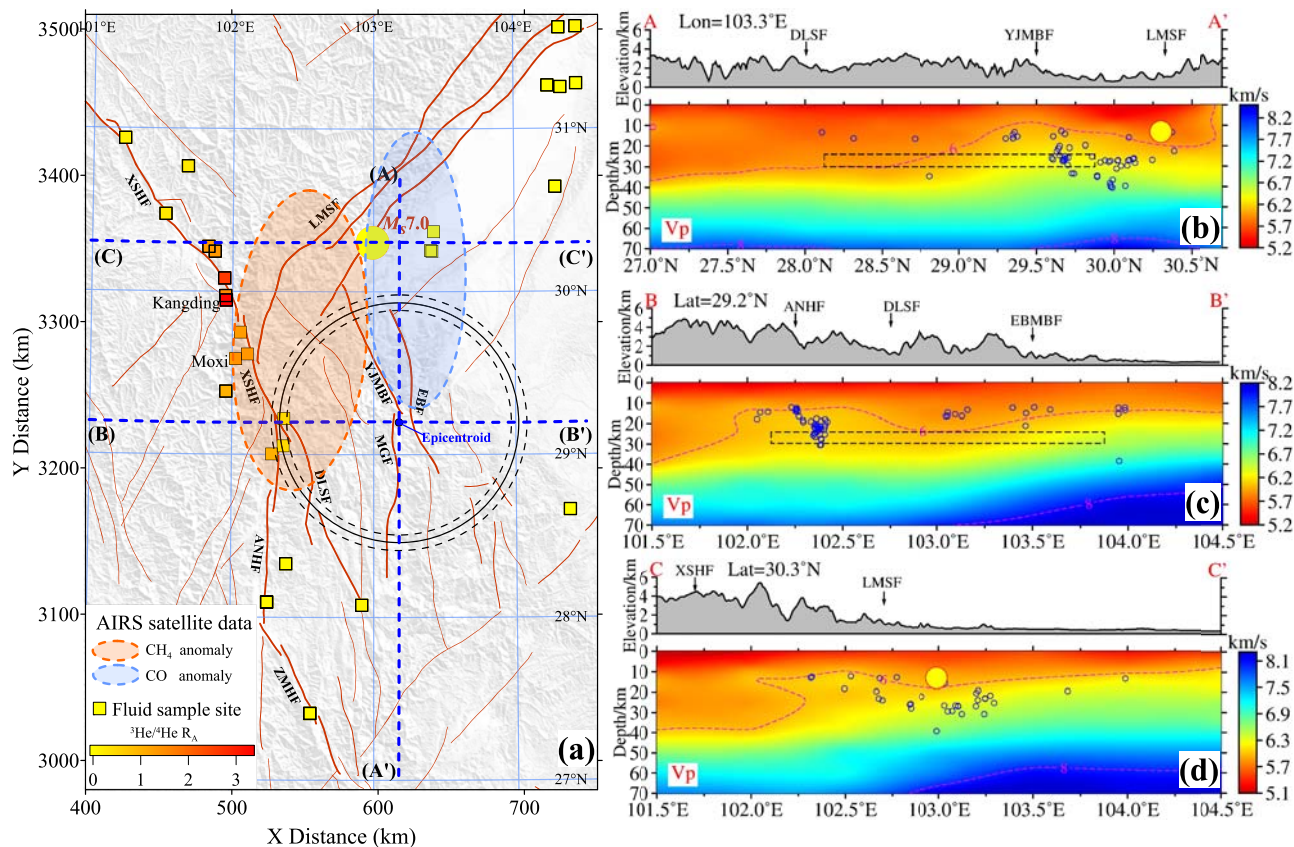
Fig. 8 ^{3}He/^{4}He, CH$_4$ and CO release area and the three velocity profiles (AA′, BB′, CC′) of crust and upper mantle. a ^{3}He/^{4}He release locations and CH$_4$, CO release areas. The square and indicate the fluid sample site. The darker the color in the square, the greater the He release. The pink and blue shaded area, respectively, outline the release area of CH$_4$ and CO. **b, c,** and **d,** respectively, indicate the velocity profiles passing through hypocentroid of the disc-shaped source model and the hypocenter of Lushan earthquake. The blue circles denote the earthquakes occurred after August 2010 as shown in Fig. 7. The yellow star represents the hypocenter of the Lushan M_S7.0 earthquake. The blue dotted box represents the longitudinal section of the disc-shaped source model.

The 2008 Wenchuan M_S8.0 earthquake accelerated strain accumulation along the LMSF southwestern segment. The 2013 Lushan M_S7.0 Earthquake that occurred in the southwest segment of the fault zone was located in the area where the strain accumulation rate accelerated and the Coulomb stress increased[23]. According to seismic imaging and stress analysis, we find that the southern part of the southern segment of the Longmenshan fault zone, near the southwest margin of the Sichuan Basin, exhibits low velocities and high Poisson's ratios[61].

Synthesis. According to above mentioned geophysical and geochemical evidence, the pre-earthquake gravity increases in the southern Lushan M_S7.0 epicenter could be caused by the large-scale deep mass migration in the source area of the M_S7.0 Lushan earthquake. Figure 9 gives an illustration of the disc-shaped source model of equivalent mass change and deep mass transfer processes before the M_S7.0 Lushan earthquake.

The tectonic converge movement between the eastern Tibet Plateau block (TPB) and the South China block (SCB)[22] enhance the local tectonic strain accumulation in the source region. As a result, the development process of micro-fractures in the middle and lower region of crust is accelerated. Then, due to the action of static rock stress, the mantle-derived fluid rich in ^{3}He/^{4}He isotopes, CH$_4$ and CO migrate upward[56]. These fluids may be re-trapped by the low-permeability layer in the crust[49,62]. This is then reflected by the gravity increase near the field source detected by the terrestrial gravity observation. A series of

numerical model experiments show that the invasion of high-pressure crustal fluids into a depth of 6–10 km can cause fast increase of gravity transient changes in the next 2–3 years[21].

Further, the mantle-derived fluid in the LVZ migrate to both sides along the horizontal direction, triggering regional seismicity anomaly[47,48]. Especially in the direction from the hypocentroid to the Lushan M_S7.0 hypocenter, the fluid migration triggers the seismicity increase like swarm activities, resulting in a wider range of the gravity increases located in the hypocentroid and adjacent region. The Fluids migration to the focal region of the Lushan earthquake could result in the lubrication of faults, activating existing structures in shallower crust and contributing to the occurrence of strong earthquakes.

Conclusions

In this study, we isolate the gravity signals potentially related to the deep mass migration. We investigate seven THRGO datasets from 2010–2013 before and after the M_S7.0 Lushan earthquake. First, we use the MBGA method to simultaneously estimate the gravimeter weights, variations of the drift rates, and scale factors of the relative gravimeter together with their uncertainties. Then, we use the BADI method to reduce the high-frequency noise effects mostly related to the local hydrological and crustal deformation and obtain the apparent density model. Finally, a parameterized disc-shaped source model is used to simulate the equivalent mass change related to the gravity change in the deep source region. Based on our observations, we propose a possible
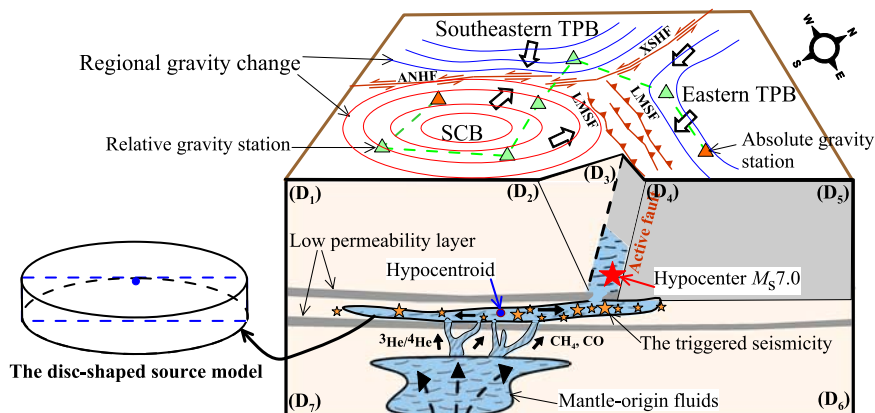
Fig. 9 The schematic diagram of disc-shaped source model and deep mass transfer process before the M_S7.0 Lushan earthquake. D_{1-7} is the cross-section of the hypocentroid and hypocenter of the M_S7.0 Lushan earthquake. The Tibet Plateau block: TPB, the South China block: SCB.

mechanism of deep mass transfer process before the Lushan M_S7.0 earthquake. The main conclusions are as follows:

(1) According to the gravity changes before the Lushan M_S7.0 earthquake, the apparent density changes range from -1.5 to $2\,\mathrm{kg\,m^{-3}}$ if the depth and thickness of the deep field source body are assumed as 13.5 km and 1 km, respectively. The model-assimilated gravity changes retrieved from this model show a trend of increasing gravity changes before the earthquake and decreasing gravity changes after the earthquake in the southern epicenter of the M_S7.0 Lushan earthquake. The gravity changes of terrestrial water change and crustal vertical deformation are about $-2\,\mu\mathrm{Gal\,yr^{-1}}$, which are not enough to explain the gravity increase up to 23 $\mu\mathrm{Gal\,yr^{-1}}$.

(2) We use a disc-shaped equivalent source model to simulate the deep mass transfer in this region. The annual rate of gravity changes is well fitted with the parameterized disc-shaped equivalent source model. The estimated disc-shaped equivalent source model has a radius of about $82 \pm 2\,\mathrm{km}$, with a thickness of about $0.7 \pm 0.1\,\mathrm{km}$ and a depth of about $26 \pm 3\,\mathrm{km}$.

(3) Geophysical and geochemical evidence supports the above results. The earthquakes with depths >10 km and magnitudes >M_S2.0 gradually move from the disk-shaped model center to the Lushan earthquake hypocenter along HLVB. The seismicity migration agrees with the assumption of fluid diffusion model with a diffusion rate of about 10 $\mathrm{m^2/s}$. The $^3\mathrm{He}/^4\mathrm{He}$ release and the abnormal increase of CH_4 release in the southern Longmenshan fault indicate the deep crustal dynamic processes in the disc-shaped area.

In conclusion, in apparent density modeling, if density variation takes up 0.18–0.74‰ of the average crustal density, it can be observed by the terrestrial time-varying gravity observation. The gravity increases before earthquake in the southern epicenter of the M_S7.0 Lushan earthquake are likely to be related to the large-scale deep crustal mass (fluids) transfer in the broad earthquake source area.

Methods

Gravity data processing and quality control. The dedicated gravity adjustment method for the continental-scale terrestrial hybrid gravity observations is a state-of-the-art technique for minimizing the effects of instrument parameter uncertainty. It is well known that the metal zero-length springs used in LaCoste and Romberg Model G gravimeters usually have an instrumental non-linear drift of tens of μGal and an instrumental scale factor that may change in time[19]. To avoid the biases caused by the instrumental drift and inaccurate scale factor, we use the Modified Bayesian gravity adjustment (MBGA) method[29,30] to process the seven THRGO datasets and obtain high-quality gravity data with uncertainty estimation

for each station and campaign. The MBGA method dedicated for the continental-scale terrestrial gravity survey can simultaneously estimate the gravimeter weights, variations of the drift rates, and scale factors of the relative gravimeter together with their uncertainties (details in Supplementary Fig. 5). The well-adjusted gravity data in this study has more reliable precision and reasonable error estimation than the original gravity dataset.

The quality control mainly includes the instrument non-linear drifts and estimated scale factors which are obtained from the absolute gravity datum (Supplementary Fig. 5a–c). For example, compared to the results obtained using the calibrated scale factors and linear drift model, the gravity values obtain using the MBGA method at the Panzhihua absolute gravity station in the four epoch observations from October 2012 to September 2013 match the results of absolute gravity measurement (Supplementary Fig. 5d) better. In general, the accuracies of gravity values at each measured stations derived from the MBGA method are within 15 μGal, and the obtained seven epochs gravity data have an average precision of 7.4 μGal.

Bayesian apparent density inversion. Many geodynamical processes can contribute to the observed gravity changes. Among them, the spatiotemporal high-frequency features are related to near-surface field sources. Therefore, the regional gravity changes potentially relate to the deep crustal source need to be isolate from the observation data. In this study, we use the Bayesian apparent density inversion (BADI) method[31,32] with spatiotemporal smoothness constraint to extract the low-frequency trend change which are potentially related to the deep crust processes. In practice, the gravity observation source noise caused by the environmental noise is assumed to obey the Gaussian distribution[63]. Based on the definition of equivalent water height in satellite gravity measurement, the BADI method employs an apparent density model to construct a relationship between the deep field source body and the surface observed gravity changes. In this method, the field source model is discretized into the tesseroids body[64]. In the absence of suitable prior constraints, the solution of gravity potential field inversion has low vertical resolution, and is not unique. Since several previous studies have found gravity changes before the M_S7.0 Lushan earthquake[26–28], we fixed the inversion depth at the focal depth. Unlike the classic gravity potential inversion method[65], the BADI method solve the non-unique problem by carrying out inversion and optimization of model parameters based on the time-varying gravity observation data under some prior constraints (Supplementary method 1).

To estimate the monitoring ability of the Sichuan gravity survey network, different sizes of tesseroid bodies have been tested (detailed in Supplementary Fig. 6). The Sichuan survey network can monitor the field sources body with a spatial resolution of $0.5^\circ \times 0.5^\circ$. Due to the uneven spatial distribution of the gravity stations, we delineate the well-resolution region of the source body in the Sichuan gravity network (outlined by the green dotted line in Supplementary Fig. 2), over which the inversion results are more accurate than the other regions. Also, we designed the forty-epochs checkerboards of theoretical gravity anomalies to further test the effect of temporal smoothness constraints (details as in Supplementary Fig. 7). Based on the actual observation, we design six epochs apparent density checkerboard to test the reliability of spatiotemporal smooth constraints for multi-period observation data (see Supplementary Fig. 8).

For the inversion of six epochs apparent density in Sichuan gravity network, the deep field source body is assumed to have a thickness of 1 km and a buried depth of 13.5 km. The tesseroid body used in this model is discretized into numerous cells, each of which has a size of $0.5^\circ \times 0.5^\circ$ in longitude and latitude.

Equivalent source model inversion. Like most gravity models, the solution to the disk model is not unique. If the density change is related to the processes that lead to earthquakes, it will certainly not be uniform in space[15]. For simplification, a

disc-shaped source model with uniform density can be used to quantify the range of the deep equivalent mass transfer. By assuming a near-horizontal detachment layer[66] at a depth of 30 km, where the behavior of the fluid layer is reasonable, we can build a forward model to estimate the observed gravity changes at the surface[20]. In this study, the disc-shaped model is used to parameterize the 'hypocentroid' and 'epicentroid' model[15,42].

Assuming that the gravity increase may be related to the deep mass migration[67,68], we estimated the positions of the ESM in the south of the Lushan earthquake. We restrict the ranges of the radius, the thickness, and the buried depth of the disc-shaped model to be 50–150 km, 1–10 km, and 10–40 km, respectively. Based on the geochemical observations, we assumed that the mass transferring in deep crust may be mainly the mantle-derived fluid rich[55–57] in $^3He/^4He$ and CH_4. The porosity also decreases with increase of depth[21]. Considering the density of $^3He/^4He$ and CH_4, we fix the equivalent density change at 1 kg m^{-3} and the rock porosity at 0.1%.

Data availability

Code availability

References

1. Van Camp, M. et al. Geophysics from terrestrial time-variable gravity measurements. *Rev. Geophys.* **55**, 938–992 (2017).
2. Battaglia, M. et al. Mass addition at Mount St. Helens, Washington, inferred from repeated gravity surveys. *J. Geophys. Res. Solid Earth* **123**, 1856–1874 (2018).
3. Tanaka, Y. et al. Gravity changes observed between 2004 and 2009 near the Tokai slow-slip area and prospects for detecting fluid flow during future slow-slip events. *Earth Planets Space* **62**, 905–913 (2010).
4. Okubo, S. Advances in gravity analyses for studying volcanoes and earthquakes. *Proc. Jpn. Acad. Ser. B* **96**, 50–69 (2020).
5. Bouih, M., Panet, I., Remy, D., Longuevergne, L. & Bonvalot, S. Deep mass redistribution prior to the 2010 Mw 8.8 Maule (Chile) Earthquake revealed by GRACE satellite gravity. *Earth Planet. Sci. Lett.* **584**, 117465 (2022).
6. Panet, I., Bonvalot, S., Narteau, C., Remy, D. & Lemoine, J.-M. Migrating pattern of deformation prior to the Tohoku-Oki earthquake revealed by GRACE data. *Nat. Geosci.* **11**, 367–373 (2018).
7. Panet, I., Narteau, C., Lemoine, J.-M., Bonvalot, S. & Remy, D. Detecting preseismic signals in GRACE gravity solutions: application to the 2011 Tohoku M$_w$ 9.0 earthquake. *J. Geophys. Res. Solid Earth* **127**, https://doi.org/10.1029/2022JB024542 (2022).
8. Wang, L. & Burgmann, R. Statistical significance of precursory gravity changes before the 2011 Mw 9.0 Tohoku-Oki earthquake. *Geophys. Res. Lett.* **46**, 7323–7332 (2019).
9. Tapley Byron, D., Bettadpur, S., Ries John, C., Thompson Paul, F. & Watkins Michael, M. GRACE measurements of mass variability in the earth system. *Science* **305**, 503–505 (2004).
10. Hinderer, J., Hector, B., Memin, A. & Calvo, M. Hybrid gravimetry as a tool to monitor surface and under ground mass changes. In *International Symposium on Earth and Environmental Sciences for Future Generations. International Association of Geodesy Symposia* (eds Freymueller, J. T. & Sánchez, L.) 123–130 (2016).
11. Van Camp, M. et al. Repeated absolute gravity measurements for monitoring slow intraplate vertical deformation in western Europe. *J. Geophys. Res.* **116**, B08402 (2011).
12. Tanaka, Y. et al. Temporal gravity anomalies observed in the Tokai area and a possible relationship with slow slips. *Earth Planets Space* **70**, 25 (2018).
13. Sun, W. et al. Gravity and GPS measurements reveal mass loss beneath the Tibetan Plateau: Geodetic evidence of increasing crustal thickness, *Geophys. Res. Lett.* 36. https://doi.org/10.1029/2008GL036512 (2009).
14. Zhu, Y., Zhan, F. B., Zhou, J., Liang, W. & Xu, Y. Gravity measurements and their variations before the 2008 Wenchuan earthquake. *Bull. Seismol. Soc. Am.* **100**, 2815–2824 (2010).
15. Chen, S. et al. Gravity increase before the 2015 Mw 7.8 Nepal earthquake. *Geophys. Res. Lett.* **43**, 111–117 (2016).
16. Xuan, S., Jin, S., Chen, Y. & Wang, J. Insight into the preparation of the 2016 MS6.4 Menyuan earthquake from terrestrial gravimetry-derived crustal density changes. *Sci. Rep.* **9**, 18227 (2019).
17. Van Camp, M., de Viron, O. & Avouac, J. P. Separating climate-induced mass transfers and instrumental effects from tectonic signal in repeated absolute gravity measurements. *Geophys. Res. Lett.* **43**, 4313–4320 (2016).
18. Yi, S., Wang, Q. & Sun, W. Is it possible that a gravity increase of 20 µGal yr^{-1} in southern Tibet comes from a wide-range density increase? *Geophys. Res. Lett.* **43**, 1481–1486 (2016).
19. Crossley, D., Hinderer, J. & Riccardi, U. The measurement of surface gravity. *Rep. Prog. Phys.* **76**, 046101 (2013).
20. Zhang, Y., Chen, S., Xing, L., Liu, M. & He, Z. Gravity changes before and after the 2008 Mw 7.9 Wenchuan earthquake at Pixian absolute gravity station in more than a decade. *Pure Appl. Geophys.* **177**, 121–133 (2020).
21. Liu, X., Chen, S. & Xing, H. Gravity changes caused by crustal fluids invasion: a perspective from finite element modeling. *Tectonophysics* **833**, 229335 (2022).
22. Xu, X. et al. Lushan MS7.0 earthquake: A blind reserve-fault event. *Chin. Sci. Bull.* **58**, 3437–3443 (2013).
23. Shan, B. et al. Stress changes on major faults caused by 2013 Lushan earthquake and its relationship with 2008 Wenchuan earthquake. *Sci. China Earth Sci.* **56**, 1169–1176 (2013).
24. Zhan, Y. et al. Deep structure beneath the southwestern section of the Longmenshan fault zone and seimogenetic context of the 4.20 Lushan MS7.0 earthquake. *Chin. Sci. Bull.*, **58**, 3467–3474 (2013).
25. Jia, K., Zhou, S., Zhuang, J. & Jiang, C. Possibility of the Independence between the 2013 Lushan Earthquake and the 2008 Wenchuan Earthquake on Longmen Shan Fault, Sichuan, China. *Seismol. Res. Lett.* **85**, 60–67 (2014).
26. Zhu, Y., Wen, X. Z., Sun, H. P. & Guo, S. S. Gravity changes before the Lushan, Sichuan, M-s = 7.0 earthquake of 2013. *Chin. J. Geophys.* **56**, 1887–1894 (2013).
27. Hao, H. et al. Gravity variation observed by scientific expedition of Lushan earthquake. *J. Geod. Geodyn.* **35**, 331–335 (2015).
28. Xuan, S., Shen, C., Li, H. & Hao, H. Characteristics of subsurface density variations before the 4.20 Lushan MS7.0 earthquake in the Longmenshan area: inversion results. *Earthq. Sci.* **28**, 49–57 (2015).
29. Chen, S., Zhuang, J., Li, X., Lu, H. & Xu, W. Bayesian approach for network adjustment for gravity survey campaign: methodology and model test. *J. Geod.* **93**, 681–700 (2019).
30. Wang, L., Chen, S., Zhuang, J. & Xu, W. Simultaneous calibration of instrument scale factor and drift rate in network adjustment for continental-scale gravity survey campaign. *Geophys. J. Int.* **228**, 1541–1555 (2022).
31. Yang, J. et al. Gravity observations and apparent density changes before the 2017 Jiuzhaigou Ms7.0 earthquake and their precursory significance. *Entropy* **23**, 1687 (2021).
32. Chen, Z. et al. Uncertainty quantification and field source inversion for the continental-scale time-varying gravity dataset: a case study in SE Tibet, China. *Pure Appl. Geophys.* https://doi.org/10.1007/s00024-022-03095-9 (2022).
33. Müller Schmied, H. et al. The global water resources and use model WaterGAP v2.2d: model description and evaluation. *Geosci. Model Dev.* **14**, 1037–1079 (2021).
34. Rodell, M. et al. The global land data assimilation system. *Bull. Am. Meteorol. Soc.* **85**, 381–394 (2004).
35. Long, D. et al. Deriving scaling factors using a global hydrological model to restore GRACE total water storage changes for China's Yangtze River Basin. *Remote Sens. Environ.* **168**, 177–193 (2015).
36. Zhang, Z., Chao, B., Chen, J. & Wilson, C. Terrestrial water storage anomalies of Yangtze river basin droughts observed by GRACE and connections with ENSO. *Glob. Planet. Change* **126**, https://doi.org/10.1016/j.gloplacha.2015.01.002 (2015).
37. Liang, S. et al. Three-dimensional velocity field of present-day crustal motion of the Tibetan Plateau derived from GPS measurements. *J. Geophys. Res. Solid Earth* **118**, 5722–5732 (2013).
38. Jiang, Z. et al. GPS constrained coseismic source and slip distribution of the 2013 Mw6.6 Lushan, China, earthquake and its tectonic implications. *Geophys. Res. Lett.* **41**, 407–413 (2014).
39. Huang, Y. et al. Fault geometry and slip distribution of the 2013 Mw 6.6 Lushan earthquake in China constrained by GPS, InSAR, leveling, and strong motion data. *J. Geophys. Res. Solid Earth* **124**, 7341–7353 (2019).
40. Chen, Y.-T., Gu, H.-D. & Lu, Z.-X. Variations of gravity before and after the Haicheng earthquake, 1975, and the Tangshan earthquake, 1976. *Phys. Earth Planet. Inter.* **18**, 330–338 (1979).
41. Kuo, J. T., Zheng, J. H., Song, S. H. & Liu, K. R. Determination of earthquake epicentroids by inversion of gravity variation data in the BTTZ region, China. *Tectonophysics* **312**, 267–281 (1999).

42. Kuo, J. T. & Yue-Feng, S. Modeling gravity variations caused by dilatancies. *Tectonophysics* **227**, 127–143 (1993).

43. Murthy, I. V. & Rao, S. J. Gravity inversion of horizontal circular discs and vertical circular cylinders. *Comput. Geosci.* **20**, 821–838 (1994).

44. Figueiredo, L., Grana, D., Roisenberg, M. & Rodrigues, B. Gaussian Mixture McMC method for linear seismic inversion. *GEOPHYSICS* **84**, 1–53 (2019).

45. Bouchon, M. et al. Extended nucleation of the 1999 Mw 7.6 Izmit earthquake. *Science* **331**, 877 (2011).

46. Kato, A. et al. Propagation of slow slip leading up to the 2011 Mw 9.0 Tohoku-Oki earthquake. *Science* **335**, 705 (2012).

47. Bräuer, K., Kämpf, H., Strauch, G. & Weise, S. M. Isotopic evidence (^{3}He/^{4}He, of fluid-triggered intraplate seismicity. *J. Geophys. Res. Solid Earth* **108**, https://doi.org/10.1029/2002JB002077 (2003).

48. Yukutake, Y. et al. Fluid-induced swarm earthquake sequence revealed by precisely determined hypocenters and focal mechanisms in the 2009 activity at Hakone volcano, Japan. *J. Geophys. Res. Solid Earth* **116**, https://doi.org/10.1029/2010JB008036 (2011).

49. Ross, Z. E., Cochran, E. S., Trugman, D. T. & Smith, J. D. 3D fault architecture controls the dynamism of earthquake swarms. *Science* **368**, 1357 (2020).

50. Enomoto, Y., Yamabe, T., Sugiura, S. & Kondo, H. Laboratory investigation of coupled electrical interaction of fracturing rock with gases. *Earth Planets Space* **73**, 90 (2021).

51. Shapiro, S. A., Huenges, E. & Borm, G. Estimating the crust permeability from fluid-injection-induced seismic emission at the KTB site. *Geophys. J. Int.* **131**, F15–F18 (1997).

52. Frassetto, A. M., Zandt, G., Gilbert, H., Owens, T. J. & Jones, C. H. Structure of the Sierra Nevada from receiver functions and implications for lithospheric foundering. *Geosphere* **7**, 898–921 (2011).

53. Abdelwahed, M. F. et al. Imaging of magma intrusions beneath Harrat Al-madinah in saudi arabia. *J. Asian Earth Sci.* **120**, 17–28 (2016).

54. Cui, Y. et al. Satellite observation of CH4 and CO anomalies associated with the Wenchuan MS 8.0 and Lushan MS 7.0 earthquakes in China. *Chem. Geol.* **469**, 185–191 (2017).

55. Geng, F., Meng, Q., Wei, M. & Lu, X. Spatio-temporal revolution characteristics of methane emission before and after the 2013 Lushan MS7.0 earthquake. *Acta Seismol. Sin.* **39**, 386–394 (2017).

56. Zhang, M. et al. Linking deeply-sourced volatile emissions to plateau growth dynamics in southeastern Tibetan Plateau. *Nat. Commun.* **12**, 4157 (2021).

57. Bao, X. et al. Two crustal low-velocity channels beneath SE Tibet revealed by joint inversion of Rayleigh wave dispersion and receiver functions. *Earth Planet. Sci. Lett.* **415**, 16–24 (2015).

58. Huang, Z. et al. Mantle structure and dynamics beneath SE Tibet revealed by new seismic images. *Earth Planet. Sci. Lett.* **411**, 100–111 (2015).

59. Hu, J. et al. Comprehensive crustal structure and seismological evidence for lower crustal flow in the southeastern margin of Tibet revealed by receiver functions. *Gondwana Res.* **55**, 42–59 (2018).

60. Liu, Y., Yao, H., Zhang, H. & Fang, H. The community velocity model V.1.0 of southwest China, constructed from joint body- and surface-wave travel-time tomography. *Seismol. Res. Lett.* **92**, 2972–2987 (2021).

61. Wang, Z., Su, J., Liu, C. & Cai, X. New insights into the generation of the 2013 Lushan Earthquake (Ms 7.0), China. *J. Geophys. Res. Solid Earth* **120**, 3507–3526 (2015).

62. Sibson, R. H. An episode of fault-valve behaviour during compressional inversion?—The 2004 MJ6.8 Mid-Niigata Prefecture, Japan, earthquake sequence. *Earth Planet. Sci. Lett.* **257**, 188–199 (2007).

63. Kennedy, J. R. & Ferré, T. P. A. Accounting for time- and space-varying changes in the gravity field to improve the network adjustment of relative-gravity data. *Geophys. J. Int.* **204**, 892–906 (2016).

64. Heck, B. & Seitz, K. A comparison of the tesseroid, prism and point-mass approaches for mass reductions in gravity field modelling. *J. Geod.* **81**, 121–136 (2007).

65. Last, B. J. & Kubik, K. Compact gravity inversion. *Geophysics* **48**, 713–721 (1983).

66. Shen, Z.-K. et al. Slip maxima at fault junctions and rupturing of barriers during the 2008 Wenchuan earthqake. *Nat. Geosci.* **2**, 718–724 (2009).

67. Wang. The raw data and datasets used in the Figs. 2–8 [Data set]. *Zenodo*. https://doi.org/10.5281/zenodo.7855090 (2023).

68. Wang. The source code of the BADI method. *Zenodo*. https://doi.org/10.5281/zenodo.7848246 (2023).

Acknowledgements

Author contributions

L.W., S.C., and J.Z. led the manuscript conceptualization, formal analysis, methodology, investigation, and writing-original draft. L.W., B.Z., W.S., J.Y., and W.X.: data curation and process, analysis and provision of materials. S.C., J.Z., and W.S. contributed the writing—review & editing.

Competing interests

The authors declare no competing interests.

Additional information

Supplementary information The online version contains supplementary material available at https://doi.org/10.1038/s43247-023-00860-z.

Correspondence and requests for materials should be addressed to Shi Chen.

Peer review information *Communications Earth & Environment* thanks Maurizio Battaglia, Jiangjun Ran and the other, anonymous, reviewer(s) for their contribution to the peer review of this work. Primary Handling Editors: Teng Wang and Joe Aslin.

Reprints and permission information is available at http://www.nature.com/reprints

Publisher's note Springer Nature remains neutral with regard to jurisdictional claims in published maps and institutional affiliations.